IEEE Photonics Journal
An IEEE Photonics Society Publication

Open Access

Bandwidth and Wavelength Tunable All-Optical Filter Based on Cascaded Opto-Mechanical Microring Resonators

Volume 11, Number 1, February 2019

Li Liu
Wei Xue
Xing Jin
Jin Yue
Zhihua Yu
Lina Zhou

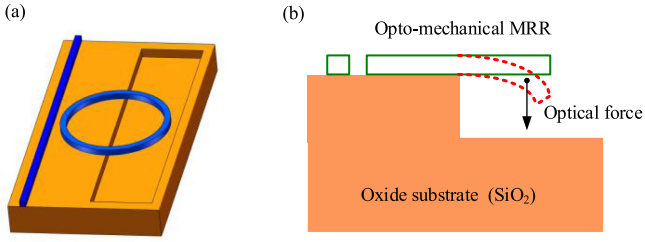

DOI: 10.1109/JPHOT.2019.2896257
1943-0655 © 2019 IEEE

IEEE photonics SOCIETY

IEEE

Bandwidth and Wavelength Tunable All-Optical Filter Based on Cascaded Opto-Mechanical Microring Resonators

Li Liu,[1,2] **Wei Xue**,[1,2] **Xing Jin**,[1,2] **Jin Yue**,[3] **Zhihua Yu**,[1,2] **and Lina Zhou**[4]

[1]School of Automation, China University of Geosciences, Wuhan 430074, China
[2]Hubei Key Laboratory of Advanced Control and Intelligent Automation for Complex Systems, Wuhan 430074, China
[3]Wuhan National Laboratory for Optoelectronics, School of Optical and Electrical Information, Huazhong University of Science and Technology, Wuhan 430074, China
[4]School of Mathematics and Physics, China University of Geosciences, Wuhan 430074, China

DOI:10.1109/JPHOT.2019.2896257

Manuscript received November 5, 2018; revised January 22, 2019; accepted January 25, 2019. Date of publication January 30, 2019; date of current version February 13, 2019. This work was supported in part by the National Natural Science Foundation of China under Grants 61805215, 11504338, and 61801063, in part by the Natural Science Foundation of Hubei Province (2018CFB167), in part by the Fundamental Research Funds for the Central Universities, in part by China University of Geosciences (Wuhan) under Grants CUG170637 and CUG2018JM15, and in part by Projects of Wuhan Science and Technology Program (2017010201010130). Corresponding author: Xing Jin (e-mail: jinxing@cug.edu.cn).

Abstract: We propose and experimentally demonstrate an all-optical filter with tunable bandwidth and wavelength based on cascaded opto-mechanical microring resonators (MRRs). As the transmission of each MRR could be tuned by injecting resonance powers, the total transmission of the three cascaded MRRs could be manipulated to realize tunable all-optical filters. Due to the free-hanging waveguides of the opto-mechanical MRRs, the nonlinear effects in the device are efficiently enhanced, which contribute to reduce the resonance powers. In the experiment, the bandwidth and wavelength tunability of the optical filter have been demonstrated by injecting three resonance powers. The tuning efficiencies of the filter's 3 dB bandwidth and wavelength could reach 0.233 nm/mW and 0.043 nm/mW respectively, which benefit the construction of all-optical systems with low-power consumptions. The footprint of the compact device is 0.02 mm^2. The proposed tunable optical filter is competent to process optical signals with dominant advantages of high tuning efficiencies, all-optical control, compact footprint, and complementary metal-oxide semiconductor-compatibility, which has significant applications for on-chip all-optical systems.

Index Terms: All-optical filter, opto-mechanical microring resonators, high-tuning efficiency.

1. Introduction

Optical filters are fundamental components of optical communication systems [1]–[3], due to their significant applications in signal quality improvement, noise suppression and wavelength division multiplexing (WDM) optical networks [4]. To process the optical signals in the next-generation reconfigurable WDM network more flexibly, optical filters with simultaneous bandwidth and wavelength tunability are highly desirable and have attracted increasing interests [5]–[7]. Widely filter approaches are based on liquid crystal modulation [8] and free space optical technology [9].

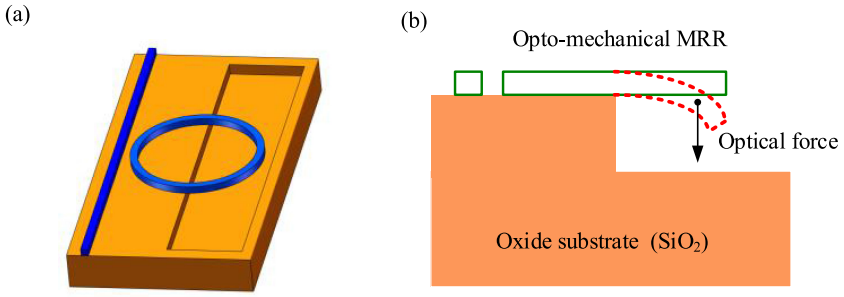

Fig. 1. (a) Schematic diagram of the opto-mechanical MRR. (b) Cross-sectional illustration of the deflected MRR influenced by the optical force.

However, such filters are complex and hard to be integrated on the silicon chip. To pursue better integration and reliability, silicon-on-insulator (SOI) technology, which possesses the advantages of high index contrast and complementary metal-oxide semiconductor (CMOS) compatibility, has become the mainstay of silicon photonics [10]–[12]. To date, several tunable optical filters based on the SOI technology have been demonstrated, such as employing the microring resonator (MRR) assisted Mach-Zehnder interferometer (MZI) structure [13], the four-tap finite impulse response structure [14], cascaded MRRs [15], cascaded Bragg-grating-assisted contra-directional couplers (DCs) [16] and the multimode Bragg grating [17]. However, these schemes mostly adopt thermal electrodes to realize the bandwidth and wavelength tunability, whose tuning efficiencies are required to be improved.

Nowadays, in order to build on-chip all-optical systems, it is urgent to realize integrated tunable all-optical filters [18]–[20]. To the best of our knowledge, there have been limited research efforts in terms of silicon all-optical filters. Therefore, an effective solution with all-optical control, high tuning efficiency and CMOS-compatibility to realize all-optical filters with bandwidth and wavelength tunability are highly desirable [21], [22].

Recently, silicon opto-mechanical MRRs have attracted widespread attentions [23]. Due to the combination of nanophotonics and nanomechanics [24], the nonlinear effects are significantly enhanced in the opto-mechanical MRRs. Through injecting low resonance powers into the opto-mechanical MRRs, their transmission characteristics could be efficiently manipulated by nonlinear effects [25], [26]. Therefore, the silicon opto-mechanical MRRs provides an energy-efficient solution for on-chip dynamic signal processing [27]–[29].

In this paper, we experimentally demonstrate an all-optical filter with tunable bandwidth and wavelength based on three cascaded silicon opto-mechanical MRRs. By injecting three resonance powers, the transfer function of the silicon device could be tuned. The experimental results demonstrate that the silicon device is competent to realize an all-optical tunable filter with high tuning efficiency. With injecting resonance powers of 1.8 mW, the bandwidth of the optical filter could be tuned from 0.89 nm to 0.47 nm. On the other hand, with injecting resonance powers of 10.24 mW, the filter wavelength could be tuned from 1552.72 nm to 1553.16 nm. Therefore, the bandwidth and wavelength tuning efficiencies could reach 0.233 nm/mW and 0.043 nm/mW, respectively. Moreover, the tuning range of the all-optical filter could be further increased by enhancing the resonance powers. The footprint of the silicon device is 0.02 mm^2. The silicon all-optical filter with high tuning efficiency and a compact footprint has significant applications for on-chip all-optical signal processing systems.

2. Operation Principle

As shown in Fig. 1(a), half waveguide of the opto-mechanical MRR is free-hanging in the air. The manipulation of the opto-mechanical MRR is based on nonlinear effects, which mainly include the thermo-optic effect and opto-mechanical effect. As the oxide substrate of the half MRR is

removed, the corresponding waveguide becomes free-hanging which significantly reduces the device heatsink. In this case, the thermo-optic effect could induce higher temperature rises and larger resonance red-shifts of the MRR. On the other hand, the opto-mechanical effect is caused by the opto-mechanical interaction between the pump light, the free-hanging MRR and the substrate [30]. As the gradient of the optical field is significantly enhanced in free-hanging MRRs, the optical force could be amplified by several orders of magnitude [31]. Thus with a low pump power, the free-hanging waveguide would be deformed downwards to the oxide substrate, which is driven by the optical force, as shown in Fig. 1(b). In this case, the effective waveguide length of the MRR would be changed which could efficiently result in resonance red-shifts. Therefore, the tuning efficiency is significantly enhanced in the opto-mechanical MRR. Though injecting lower pump powers into the opto-mechanical device, larger resonance red-shifts could be realized.

The resonance red-shift $\delta\lambda_1$ caused by the thermo-optic effect could be written as [32]

$$\delta\lambda_1 \approx \frac{\lambda_r}{n_g} R_{\text{th}} k_{\text{th}} \Gamma_{\text{th}} P_t \tag{1}$$

where λ_r is the resonant wavelength, n_g is the group index, R_{th} is the thermal resistance of the silicon ring resonator, k_{th} is silicon thermo-optic coefficient, Γ_{th} is the effective confinement factor, and P_t is the optical pump power for the thermo-optic effect.

On the other hand, the resonance red-shift $\delta\lambda_2$ caused by the opto-mechanical effect can be given by [33]

$$\delta\lambda_2 \propto g_{om}^2 \cdot P_m / k \tag{2}$$

where $g_{om} = \frac{\partial n_{eff}}{\partial g}$ is the opto-mechanical tuning efficiency, n_{eff} is the effective index of the free-hanging MRR, g represents the waveguide separation between the free-hanging arc and the substrate, P_m is the circulating pump power on the ring for the opto-mechanical effect, and k is the beam stiffness.

Therefore, the total resonance red-shift $\delta\lambda$ can be determined by

$$\delta\lambda = \delta\lambda_1 + \delta\lambda_2 \propto P_{\text{in}} \tag{3}$$

where P_{in} is the input power of λ_r which mainly consists of P_t and P_m. It is clear that the MRR resonance red-shifts are proportional to the input pump power P_{in}. Thus the transmission of the opto-mechanical MRR could be efficiently manipulated by adjusting the input pump powers. Because the coupling efficiencies of the MRR resonances are higher, the pump light aligned at the resonances could cause the larger resonance red-shifts.

The device consists of three cascaded opto-mechanical MRRs (i.e., R_1, R_2 and R_3) with different radii, as shown in Fig. 2(a). The waveguide structures in the blue dashed boxes are free-hanging arcs. The six resonant wavelengths belong to R_1(λ_{1a} and λ_{1b}), R_2(λ_{2a} and λ_{2b}) and R_3(λ_{3a} and λ_{3b}), respectively. The pump powers of three resonances λ_{1b}, λ_{2b} and λ_{3b} are utilized to activate the nonlinear effects in the corresponding MRR and then the other three resonances (i.e., λ_{1a}, λ_{2a} and λ_{3a}) could be accordingly shifted. The resonances λ_{1b} and λ_{3b} are injected from port 1 while λ_{2b} is injected from port 2.

Due to the Vernier effect, the device transmission spectrum is illustrated as the green solid line in Fig. 2(b). The first and second free spectral ranges (FSRs) are used as the filter region (i.e., λ_{1a}, λ_{2a} and λ_{3a}) and pump region (i.e., λ_{1b}, λ_{2b} and λ_{3b}), respectively. Namely, the pump powers of λ_{1b}, λ_{2b} and λ_{3b} are employed to manipulate the transmission characteristics of the filter region. The bandwidth tuning principle of the all-optical filter is shown in Fig. 2(c). Firstly, without pump power, the transfer function of the optical filter is unchanged which is shown as the green line. According to Eq. (3), the MRR resonance red-shifts are proportional to the input pump powers. Then, the pump power of λ_{2b} is turned on while the other two pump powers are still turned off. The initial resonance λ_{2a} could be shifted to λ_{2c}, which is shown as the red dashed line in Fig. 2(c). In this case, the 3dB-bandwidth (BW) of the optical filter could realize the maximum value of BW_{max}. Finally, by simultaneously turning on and adjusting the pump powers of λ_{1b} and λ_{2b}, the initial resonances λ_{1a} and λ_{2a} could be shifted in order to overlap with λ_{3a}, which is shown as the blue dashed line in Fig. 2(c). As a result, the BW of the optical filter could achieve the minimum value of BW_{min}.

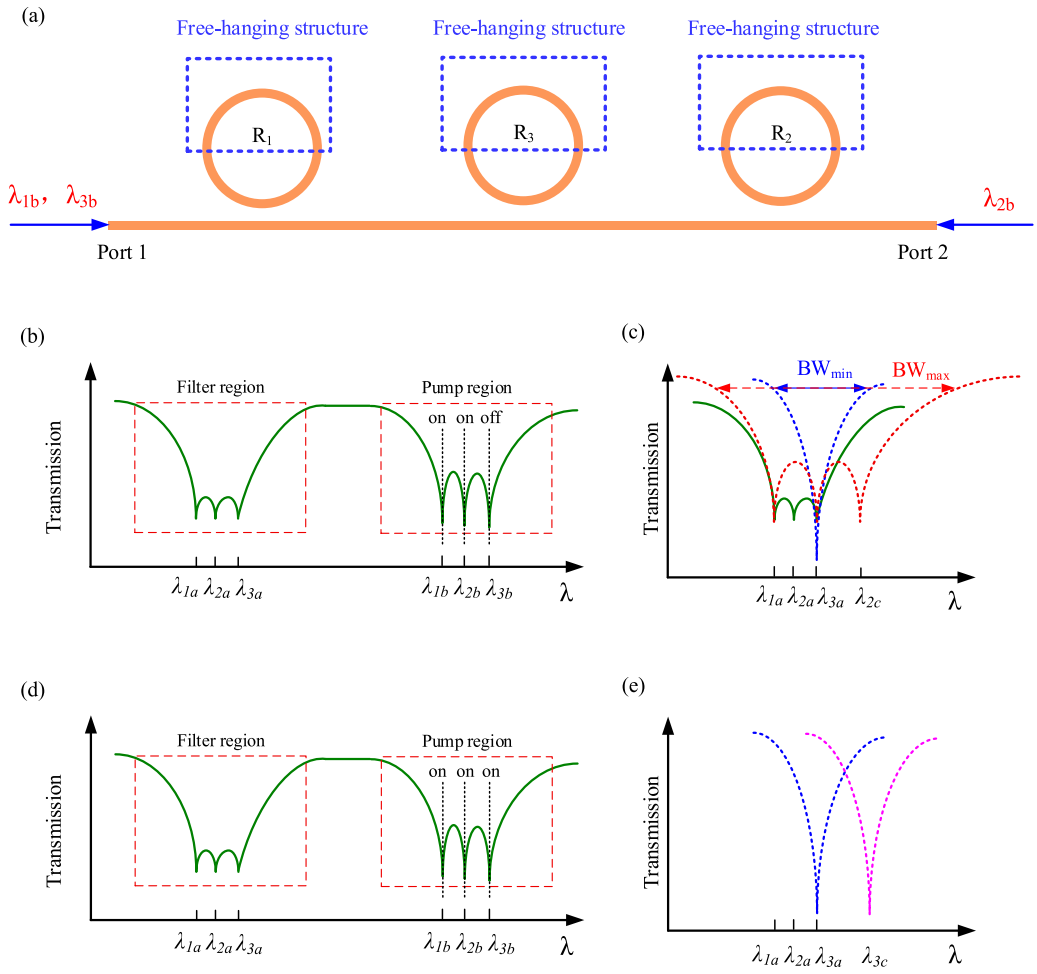

Fig. 2. (a) The device structure of the optical filter. (b) and (d) are the pump conditions for bandwidth tunability and wavelength tunability, respectively. (c) and (e) are the tuning range of bandwidth and wavelength, respectively.

Therefore, the BW of the all-optical filter could be tuned from BW_{min} to BW_{max} by adjusting the powers in the pump region (i.e., λ_{1b} and λ_{2b}).

Figures 2(d) and 2(e) illustrate the tuning process of the filter wavelength. As discussed in Fig. 2(c), the optical filter with the wavelength of λ_{3a} (blue dashed line) has been achieved by injecting two pump powers of λ_{1b} and λ_{2b}. Then, the powers in the pump region (λ_{1b}, λ_{2b} and λ_{3b}) are all turned on and injected into the device, as shown in Fig. 2(d). By adjusting the three pump powers, the three resonances in the filter region (λ_{1a}, λ_{2a} and λ_{3a}) could all be tuned to λ_{3c}. In this case, the wavelength of the optical filter could be tuned from λ_{3a} (the blue dashed line) to λ_{3c} (the pink dashed line) in Fig. 2(e). Therefore, the wavelength of the all-optical filter could also be tuned by manipulating the three powers in the pump region (i.e., λ_{1b}, λ_{2b} and λ_{3b}).

Finite element analysis and waveguide theory are used to design the device parameters. By utilizing the finite-difference time-domain (FDTD) method [34], [35], the MRR bending loss could be negligible when the ring radius is larger than 5 μm. Considering the practical fabrication technology and waveguide single-mode transmission, the radius and waveguide width of the MRR are designed around 20 μm and 450 nm, respectively. Subsequently, the waveguide modes are simulated by the finite-element mode solver [36]. As the silicon slab of SOI wafer is 220 nm, the filter slab height is designed as 30 nm to realize ridge waveguides. In this case, the differences of the waveguide

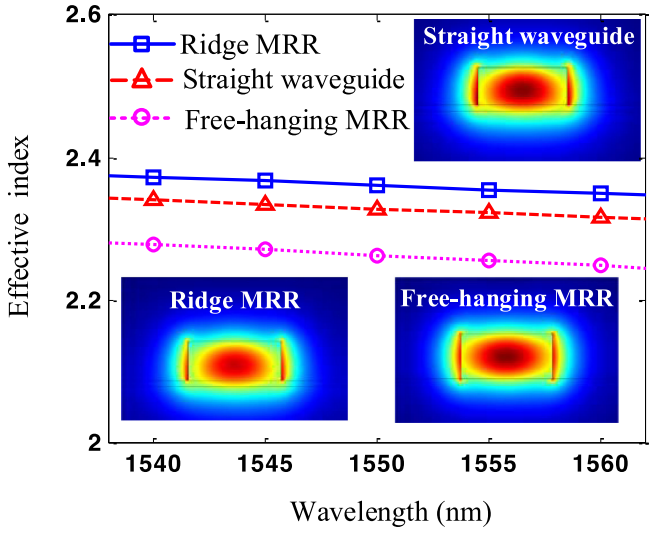

Fig. 3. Effective indexes and energy profiles of the fundamental modes in different waveguide structures.

effective indexes could be negligible, which benefits the signal transmission and mode coupling between different waveguide structures. Figure 3 shows that the effective indexes of the ridge MRR (blue solid line), straight waveguide (red dashed line) and free-hanging MRR (pink dotted line) at 1550 nm are 2.36, 2.33 and 2.26, respectively. The energy profiles of the fundamental modes in the ridge MRR, free-hanging MRR and straight waveguide are shown as the inset images. Therefore, the parameters of the silicon MRRs could be designed by finite element analysis to optimize the device performances (e.g., resonant wavelengths and bandwidths).

In order to experimentally demonstrate the all-optical tunable filters, the cascaded opto- mechanical MRRs were fabricated on an SOI wafer with a 220-nm-thick top silicon layer and a 2-μm-thick buried oxide layer through a CMOS compatible process. Through three production steps, the free-hanging waveguides of the MRRs could be released by selective etching processing. At first, the whole device was transferred to photoresist by the first E-beam lithography (EBL) and then etched downwards for 190 nm through the first inductively coupled plasma (ICP) etching. At this time, the device became a structure of ridge waveguides. Secondly, only half of each MRR was etched downwards for another 30 nm by the second EBL and ICP etching in order to realize the slab waveguide structure. In this case, the oxide substrates around the above slab waveguides were exposed to the air. Namely, a corrosion window for the later hydrofluoric (HF) etching was built while the other half of each MRR with a 30-nm-thick silicon layer would be protected from the HF etching. Finally, the HF acid etching was used to selectively etch the oxide substrate in the corrosion window region. In this case, the half waveguide of each opto-mechanical MRR was free-hanging while the other waveguides were fixed. Through the above three steps, the opto-mechanical device was fabricated. Due to the different etched depths, the effect of Fresnel-reflection might slightly increase the device loss. Compared to the normal MRR, the extra loss of the free-hanging MRR is about 0.5 dB.

Figure 4(a) shows the scanning electron microscope (SEM) image of the silicon device (i.e., R_1, R_2 and R_3). The footprint of the whole device is 0.02 mm^2. The radii of the three MRRs are about 20 μm (R_1), 20.06 μm (R_2) and 20.12 μm (R_3), respectively. The waveguides in the yellow dashed boxes are the free-hanging arcs. As the separation distance among the cascaded MRRs is about 55 μm, the thermal influence between the three MRRs could be negligible. The zoom-in image of R_1 is shown in Fig. 4(b). The coupling gap between the ring and the straight waveguide is 200 nm. To ensure single-mode transmission, the waveguide width of the free-hanging MRR was 450 nm, as shown in Fig. 4(c).

The transmission spectrum of the silicon device is shown in Fig. 5(a). The FSR is about 4.5 nm. According to the operation principle in Fig. 2(b), the first FSR and the third FSR are chosen as

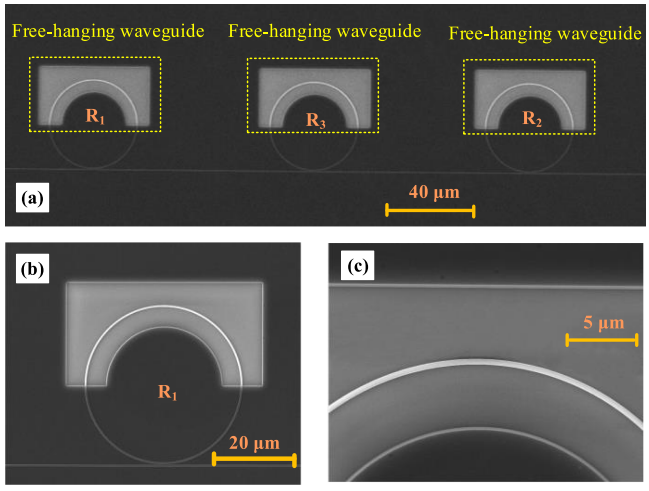

Fig. 4. (a) The SEM image of the cascaded opto-mechanical MRRs. (b) The SEM image of R_1. (c) The zoom-in region of the free-hanging structure.

the pump region and the filter region, respectively. Figure 5(b) shows the spectrum of the filter region with an extinction ratio of 36 dB. The wavelength of the resonance λ_{1a} is 1552.54 nm and the wavelengths of the other two resonances λ_{2a} and λ_{3a} are around 1552.7 nm. As shown in Fig. 5(c), the wavelengths of the three resonances (λ_{1b}, λ_{2b} and λ_{3b}) in the pump region are 1543.46 nm, 1543.576 nm and 1543.69 nm, respectively. The tuning characteristics of the device is also measured, as shown in Fig. 5(d). Through injecting different pump powers of λ_{1b}, λ_{2b} and λ_{3b}, the resonance red-shifts of the corresponding MRR are illustrated as the red solid line (R_1), the blue dashed line (R_2) and the green dotted line (R_3), respectively. It is clear that the resonance red-shifts increase linearly with the corresponding pump powers, which are efficient to realize tunable filters. For example, the resonance red-shift of R_1 is larger than 0.3 nm while injecting a pump power of 2 mW.

3. Experimental Results

In order to demonstrate the bandwidth tunability of the all-optical filter, two pump powers (P_1 at λ_{1b} and P_2 at λ_{2b}) are injected into the silicon device. In this case, the corresponding two resonances λ_{1a} and λ_{2a} would be shifted while the other resonance λ_{3a} remains unchanged. Meanwhile, a low-power amplified spontaneous emission (ASE) source is coupled with the pump powers to characterize the device transmission spectrum.

The initial spectrum of the filter region is shown as the black line in Fig. 6(a). Firstly, the two pump powers (P_1 and P_2) are set as 0 mW and 1.8 mW, respectively. Under the influence of the nonlinear effects, the resonance λ_{2a} shifts to 1552.94 nm. In this case, the measured filter spectrum is shown as the blue line. As a result, the optical filter could realize a maximum 3 dB-bandwidth of 0.89 nm with an ER around 20 dB. Secondly, the pump power P_1 is enhanced to 0.42 mW so as to increase the red-shift of λ_{1a}, while P_2 is reduced to 1.35 mW to decrease the red-shift of λ_{2a}. In this case, the two resonances shift to 1552.62 nm (λ_{1a}) and 1552.86 nm (λ_{2a}), respectively. The pink curve shows the filter spectrum with a 3dB-bandwidth of 0.72 nm. Thirdly, the two pump powers (P_1 and P_2) are set as 0.78 mW and 1.03 mW, in order to shift the two resonances to 1552.66 nm (λ_{1a}) and 1552.82 nm (λ_{2a}), respectively. The measured filter spectrum is shown as the green line and the filter's 3 dB-bandwidth is 0.61 nm. Finally, the pump power P_1 is increased to 0.95 mW while P_2 is decreased to 0.51 mW, respectively. Accordingly, the two resonances λ_{1a} and λ_{2a} are both shifted around λ_{3a} (i.e., 1552.7 nm). In this case, the 3dB-bandwidth of the optical filter could realize a minimum value of 0.47 nm with a large ER of 48 dB.

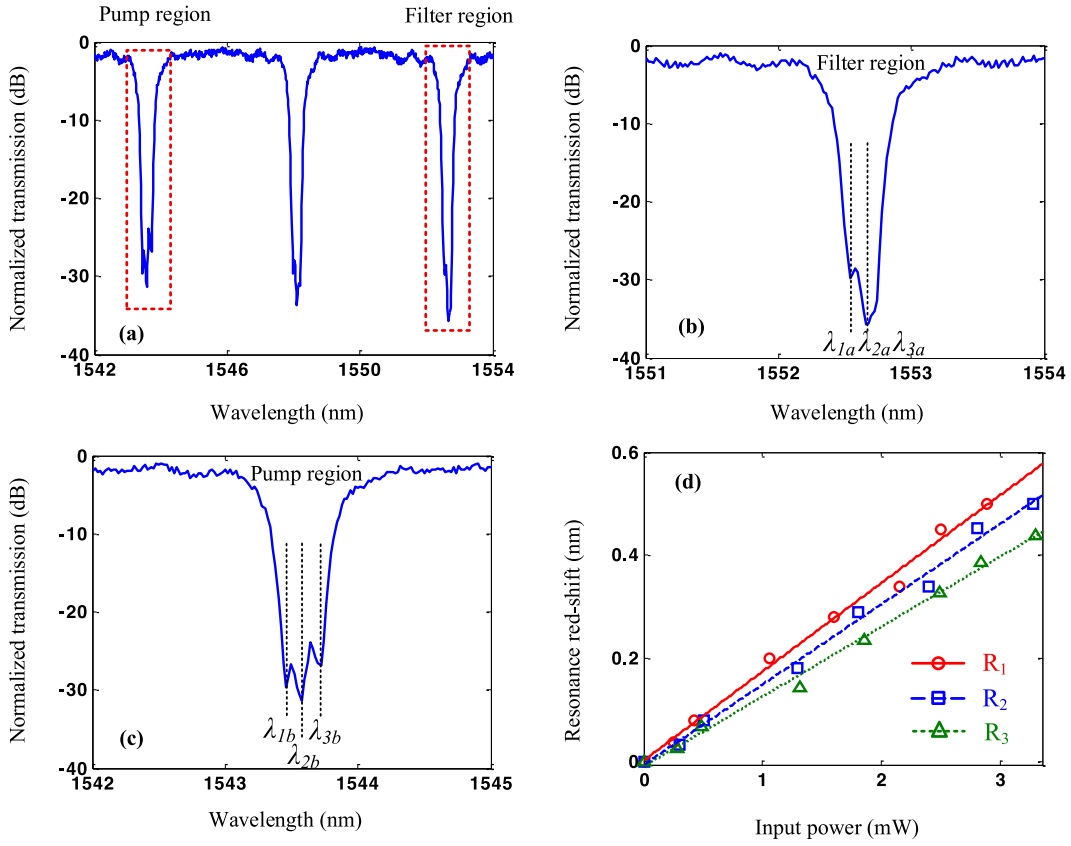

Fig. 5. (a) The transmission spectrum of the cascaded MRRs. (b) The filter region. (c) The pump region. (d) The measured resonance red-shifts when injecting different pump powers.

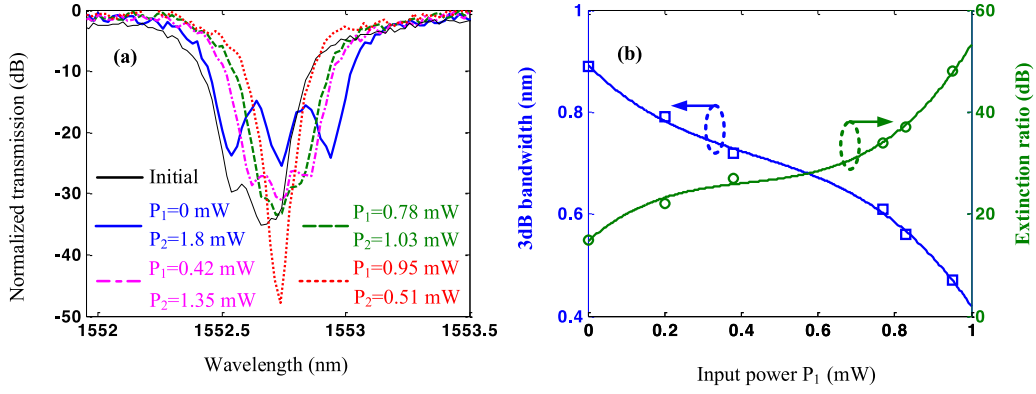

Fig. 6. (a) The measured spectra of the optical filter with tunable 3 dB-bandwidth. (b) The varied 3 dB-bandwidths and extinction ratios under different pump powers.

Figure 6(b) shows the 3dB-bandwidths (blue line) and extinction ratios (green line) of the optical filter when affected by different pump powers (i.e., P_1 and P_2). By adjusting P_1 from 0 mW to 0.95 mW and P_2 from 1.8 mW to 0.51 mW, the 3dB-bandwidth of the optical filter could be tuned from 0.89 nm to 0.47 nm. Therefore, the tuning efficiency of the filter's 3dB-bandwidth expressed as BW/P_{max} is 0.233 nm/mW. The extinction ratios of the filter varies from 18 dB to 48 dB, which is shown as the green line.

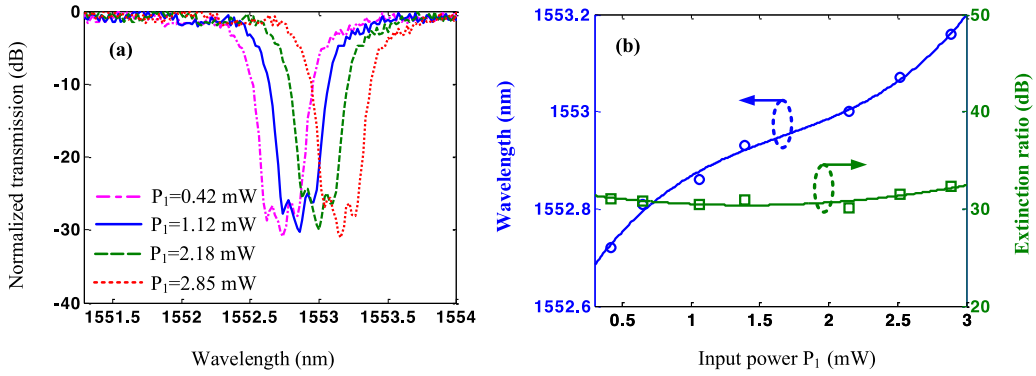

Fig. 7. (a) The measured spectra of the optical filter with tunable wavelength. (b) The varied wavelengths and extinction ratios under different pump powers.

TABLE 1
Performance Comparisons of Recent Silicon-Based Optical Filters

Device	Bandwidth tuning efficiency (nm/mW)	Wavelength tuning efficiency (nm/mW)
MZI+MRRs [13]	0.025	0.042
MZI+PM [14]	0.004	0.003
Cascaded MRRs [15]	0.023	0.030
Cascaded contra-DCs [16]	0.042	0.023
Multimode Bragg grating [17]	0.050	0.025
This work	0.233	0.043

To further investigate the wavelength tunability of the optical filter, we have chosen the transfer function shown as the pink dotted dashed curve in Fig. 6(a). In this case, the central wavelength of the optical filter is around 1552.7 nm. The corresponding pump powers are $P_1 = 0.42$ mW, $P_2 = 1.35$ mW and P_3 at λ_{3a} is 0 mW. Then, by adjusting the three pump powers, the central wavelengths of the optical filter could be tuned to 1552.86 nm ($P_1 = 1.12$ mW, $P_2 = 2.16$ mW, $P_3 = 1.28$ mW), 1553.0 nm ($P_1 = 2.18$ mW, $P_2 = 3.12$ mW, $P_3 = 2.36$ mW) and 1553.16 nm ($P_1 = 2.85$ mW, $P_2 = 3.86$ mW, $P_3 = 3.53$ mW), respectively. Therefore, with the maximum pump power of 10.24 mW, Fig. 7(a) shows that the central wavelength of the optical filter could be tuned from 1552.72 nm to 1553.16 nm. Thus, the tuning efficiency of the filter wavelength is 0.043 nm/mW. As shown in Fig. 7(b), the variation of the filter wavelengths and ERs are shown as the blue line and green line, respectively. The maximum tuning range of the filter wavelengths could realize 0.44 nm with ERs larger than 30 dB. By enhancing the pump powers, the tuning range of the filter wavelengths could be further increased. Moreover, in order to investigate the stability of the optical filter, we have measured the central wavelengths of the optical filter at different times. Within six hours, the maximum shift of the filter central wavelengths is 0.03 nm, which could be negligible due to the wavelength magnitude of 1550 nm. If the environmental conditions (e.g., ambient temperature) can be controlled, the performance of the optical filter will be stable.

Table 1 illustrates the tuning performances of recent optical filters on silicon platforms. Two major parameters of the filters (i.e., bandwidth tuning efficiency and wavelength tuning efficiency) are compared by using different silicon structures. Due to the advantages of the opto-mechanical

MRRs, the tuning efficiencies of the filter bandwidth and wavelength in this work are much larger than the other schemes. Especially, the bandwidth tuning efficiency has been significantly improved to a high value of 0.233 nm/mW. Moreover, the optical filter in this work is tuned in the all-optical field that benefits the building of an all-optical system. Therefore, with the dominant advantages of high tuning efficiencies, a compact size and all-optical control, the proposed silicon optical filter is significantly superior for usage in on-chip signal processing.

As the tuning results of the optical filter are mainly determined by the characteristics of the silicon opto-mechanical MRRs, the performances could be significantly improved by optimizing the device structures and parameters. Firstly, the nonlinear effects in the opto-mechanical MRRs could be enhanced by optimizing the separation gap between the oxide substrate and the free-hanging arc [37], [38]. In this case, the required pump powers could be reduced and the tuning efficiencies would be accordingly increased. Secondly, the coupling gaps between the MRRs and the straight waveguides could be optimized to realize the critical coupling. Thus, the extinction ratios of the optical filter could be improved [39], [40]. Furthermore, better fabrication technology [41] and post-processing technology [42] could be employed to reduce the device transmission loss and pump powers, which would also improve the tuning efficiencies.

4. Conclusions

In conclusion, we have experimentally demonstrated an all-optical tunable filter with high tuning efficiencies based on silicon opto-mechanical MRRs, which could be driven by low resonance powers. The tuning efficiencies of the filter 3dB-bandwidth and wavelength could reach 0.233 nm/mW and 0.043 nm/mW, respectively. Moreover, the tuning range of the all-optical filter could be further increased by enhancing the resonance powers. The footprint of the whole device is 0.02 mm^2. Our scheme provides an all-optical tunable filter of CMOS-compatibility, a compact footprint and high tuning efficiencies which has many significant applications for on-chip all-optical signal processing.

References

[1] M. S. Rasras *et al.*, "Demonstration of a fourth-order pole-zero optical filter integrated using CMOS processes," *J. Lightw. Technol.*, vol. 25, no. 1, pp. 87–92, Jan. 2007.

[2] F. Xia, M. Rooks, L. Sekaric, and Y. Vlasov, "Ultra-compact high order ring resonator filters using submicron silicon photonic wires for on-chip optical interconnects," *Opt. Exp.*, vol. 15, no. 19, pp. 11934–11941, 2007.

[3] A. d'Alessandro *et al.*, "Tunable integrated optical filter made of a glass ion-exchanged waveguide and an electro-optic composite holographic grating," *Opt. Exp.*, vol. 16, no. 13, pp. 9254–9260, 2008.

[4] I. Papagiannakis *et al.*, "Investigation of 10-Gb/s RSOA-based upstream transmission in WDM-PONs utilizing optical filtering and electronic equalization," *IEEE Photon. Technol. Lett.*, vol. 20, no. 24, pp. 2168–2170, Dec. 2008.

[5] Y. Jiang *et al.*, "A selectable multiband bandpass microwave photonic filter," *IEEE Photon. J.*, vol. 5, no. 3, Jun. 2013, Art. no. 5500509.

[6] P. B. Deotare *et al.*, "All optical reconfiguration of optomechanical filters," *Nature Commun.*, vol. 3, 2012, Art. no. 846.

[7] J. Yao and M. C. Wu, "Bandwidth-tunable add-drop filters based on micro-electro-mechanical-system actuated silicon microtoroidal resonators," *Opt. Lett.*, vol. 34, no. 17, pp. 2557–2559, 2009.

[8] Y. Huang and S. Zhang, "Optical filter with tunable wavelength and bandwidth based on cholesteric liquid crystals," *Opt. Lett.*, vol. 36, no. 23, pp. 4563–4565, 2011.

[9] E. Torrengo *et al.*, "Transoceanic PM-QPSK terabit superchannel transmission experiments at baud-rate subcarrier spacing," in *Proc. Eur. Conf. Opt. Commun.*, 2010, paper We.7.C.2.

[10] L. Liu, J. Dong, and X. Zhang, "Chip-integrated all-optical 4-bit Gray code generation based on silicon microring resonators," *Opt. Exp.*, vol. 23, no. 16, pp. 21414–21423, 2015.

[11] J. Leuthold, C. Koos, and W. Freude, "Nonlinear silicon photonics," *Nature Photon.*, vol. 4, no. 8, pp. 535–544, 2010.

[12] L. Liu, J. Yue, and Z. Li, "All-optical switch based on a fiber-chip-fiber opto-mechanical system with ultrahigh extinction ratio," *IEEE Photon. J.*, vol. 9, no. 3, Jun. 2017, Ar. no. 7104208.

[13] Y. Ding *et al.*, "Bandwidth and wavelength tunable optical bandpass filter based on silicon microring-MZI structure," *Opt. Exp.*, vol. 19, no. 7, pp. 6462–6470, 2011.

[14] S. Liao, Y. Ding, C. Peucheret, T. Yang, J. Dong, and X. Zhang, "Integrated programmable photonic filter on the silicon-on-insulator platform," *Opt. Exp.*, vol. 22, no. 26, pp. 31993–31998, 2014.

[15] T. Dai *et al.*, "Bandwidth and wavelength tunable optical passband filter based on silicon multiple microring resonators," *Opt. Lett.*, vol. 41, no. 20, pp. 4807–4810, 2016.

[16] J. St-Yves, H. Bahrami, P. Jean, S. LaRochelle, and W. Shi, "Widely bandwidth-tunable silicon filter with an unlimited free-spectral range," *Opt. Lett.*, vol. 40, no. 23, pp. 5471–5474, 2015.

[17] J. Jiang *et al.*, "Broadband tunable filter based on the loop of multimode Bragg grating," *Opt. Exp.*, vol. 26, no. 1, pp. 559–566, 2018.
[18] Y. Zheng, Q. Yu, K. Tao, and Z. Ouyang, "All-optical tunable filters based on optomechanical effects in two-dimensional photonic crystal cavities," *Opt. Lett.*, vol. 38, no. 21, pp. 4362–4365, 2013.
[19] H. Nasari and M. S. Abrishamian, "All-optical tunable notch filter by use of kerr nonlinearity in the graphene microribbon array," *J. Opt. Soc. Amer. B*, vol. 31, no. 7, pp. 1691–1697, 2014.
[20] A. E. Willner, S. Khaleghi, M. R. Chitgarha, and O. F. Yilmaz, "All-optical signal processing," *J. Lightw. Technol.*, vol. 32, no. 4, pp. 660–680, Feb. 2014.
[21] H. Yu *et al.*, "All-optical full-band RF receiver based on an integrated ultra-high-Q bandpass filter," *J. Lightw. Technol.*, vol. 34, no. 2, pp. 701–706, Jan. 2016.
[22] B. Cai *et al.*, "Integrated tunable all-optical filters based on push-pull fractional order photonics Hilbert transformers," in *Proc. Asia Commun. Photon. Conf.*, 2016, paper AS3F-4.
[23] L. Liu, Y. Yang, Z. Li, X. Jin, W. Mo, and X. Liu, "Low power consumption and continuously tunable alloptical microwave filter based on an opto-mechanical microring resonator," *Opt. Exp.*, vol. 25, no. 2, pp. 960–971, 2017.
[24] M. Ren *et al.*, "Nano-optomechanical actuator and pull-back instability," *ACS Nano*, vol. 7, no. 2, pp. 1676–1681, 2013.
[25] L. Liu, H. Qiu, Z. Chen, and Z. Yu, "Photonic measurement of microwave frequency with low-error based on an optomechanical microring resonator," *IEEE Photon. J.*, vol. 9, no. 6, Dec. 2017, Art. no. 5503511.
[26] Y. Shi *et al.*, "Nanometer-precision linear sorting with synchronized optofluidic dual barriers," *Sci. Adv.*, vol. 4, no. 1, 2018, Art. no. eaao0773.
[27] B. Dong *et al.*, "A nanoelectromechanical systems actuator driven and controlled by Q-factor attenuation of ring resonator," *Appl. Phys. Lett.*, vol. 103, no. 18, 2013, Art. no. 181105.
[28] Y. Z. Shi *et al.*, "Sculpting nanoparticle dynamics for single-bacteria-level screening and direct binding-efficiency measurement," *Nature Commun.*, vol. 9, no. 1, 2018, Art. no. 815.
[29] Y. Z. Shi *et al.*, "High-resolution and multi-range particle separation by microscopic vibration in an optofluidic chip," *Lab Chip*, vol. 17, no. 14, pp. 2443–2450, 2017.
[30] D. Van Thourhout and J. Roels, "Optomechanical device actuation through the optical gradient force," *Nature Photon.*, vol. 4, no. 4, pp. 211–217, 2010.
[31] L. Liu *et al.*, "Low-power all-optical microwave filter with tunable central frequency and bandwidth based on cascaded opto-mechanical microring resonators," *Opt. Exp.*, vol. 25, no. 15, pp. 17329–17342, 2017.
[32] M. Xu, J. Wu, T. Wang, X. Hu, X. Jiang, and Y. Su, "Push-pull optical nonreciprocal transmission in cascaded silicon microring resonators," *IEEE Photon. J.*, vol. 5, no. 1, Feb. 2013, Art. no. 2200307.
[33] H. Cai *et al.*, "A nanoelectromechanical systems optical switch driven by optical gradient force," *Appl. Phys. Lett.*, vol. 102, no. 2, 2013, Art. no. 023103.
[34] Z. Sheng, D. Dai, and S. He, "Comparative study of losses in ultrasharp silicon-on-insulator nanowire bends," *IEEE J. Sel. Topics Quantum Electron.*, vol. 15, no. 5, pp. 1406–1412, Sep./Oct. 2009.
[35] L. Liu, J. Yue, X. Fan, and W. Xue, "On-chip passive optical diode with low-power consumption," *Opt. Exp.*, vol. 26, no. 25, pp. 33463–33472, 2018.
[36] Z. Huang *et al.*, "Strong optomechanical coupling in nanobeam cavities based on hetero optomechanical crystals," *Sci. Rep.*, vol. 5, 2015, Art. no. 15964.
[37] Y. Long and J. Wang, "Optically-controlled extinction ratio and Q-factor tunable silicon microring resonators based on optical forces," *Sci. Rep.*, vol. 4, 2014, Art. no. 5409.
[38] L. Midolo, A. Schliesser, and A. Fiore, "Nano-opto-electro-mechanical systems," *Nature Nanotechnol.*, vol. 13, no. 1, pp. 11–18, 2018.
[39] Y. Zhang *et al.*, "Silicon optical diode based on cascaded photonic crystal cavities," *Opt. Lett.*, vol. 39, no. 6, pp. 1370–1373, 2014.
[40] L. Liu, J. Dong, D. Gao, A. Zheng, and X. Zhang, "On-chip passive three-port circuit of all-optical ordered-route transmission," *Sci. Rep.*, vol. 5, no. 1, 2015, Art. no. 10190.
[41] A. Biberman, M. J. Shaw, E. Timurdogan, J. B. Wright, and M. R. Watts, "Ultralow-loss silicon ring resonators," *Opt. Lett.*, vol. 37, no. 20, pp. 4236–4238, 2012.
[42] L. Martinez and M. Lipson, "High confinement suspended micro-ring resonators in silicon-on-insulator," *Opt. Exp.*, vol. 14, no. 13, pp. 6259–6263, 2006.